Soliton generation and multiple phases in dispersive shock and rarefaction wave interaction

M. J. Ablowitz and D. E. Baldwin*
Department of Applied Mathematics, University of Colorado, Boulder, Colorado 80309-0526, USA

M. A. Hoefer
Department of Applied Physics and Applied Mathematics, Columbia University, New York, New York 10027, USA

(Received 26 February 2009; revised manuscript received 27 April 2009; published 16 July 2009)

Interactions of dispersive shock waves (DSWs) and rarefaction waves (RWs) associated with the Korteweg–de Vries equation are shown to exhibit multiphase dynamics and isolated solitons. There are six canonical cases: one is the interaction of two DSWs that exhibit a transient two-phase solution but evolve to a single-phase DSW for large time; two tend to a DSW with either a small amplitude wave train or a finite number of solitons, which can be determined analytically; two tend to a RW with either a small wave train or a finite number of solitons; finally, one tends to a pure RW.

DOI: 10.1103/PhysRevE.80.016603 PACS number(s): 05.45.Yv, 47.40.Nm, 52.35.Mw

Shock waves in processes dominated by weak dispersion and nonlinearity have been experimentally observed in plasmas [1], water waves [2], and more recently in Bose-Einstein condensates [3,4] and nonlinear optics [5]; these dispersive shock waves (DSWs) have yielded novel dynamics and interesting interaction behavior, which has only recently begun to be studied theoretically (cf. [6,7]). Here we consider DSWs that are described by the Korteweg–de Vries (KdV) equation

$$u_t + uu_x + \varepsilon^2 u_{xxx} = 0, \quad 0 < \varepsilon \ll 1. \tag{1}$$

Individual DSWs are characterized by a soliton train front with an expanding oscillatory wave at its trailing edge; these waves have been well studied (cf. [8,9]) using wave averaging techniques, often referred to as Whitham theory [10,11].

When illustrative, we contrast DSW interaction with classical or viscous shock waves (VSWs), which are dominated by weak *dissipation* and nonlinearity, using Burgers' equation

$$u_t + uu_x - \nu u_{xx} = 0, \quad 0 < \nu \ll 1. \tag{2}$$

The interaction of VSWs is an entire field and has been extensively studied (cf. [12]), while little is known about DSW interactions.

In this paper, we use analytic, asymptotic, and numeric methods to investigate Eqs. (1) and (2) using the "steplike" initial data

$$u(x,0) = u_0(x) = \begin{cases} h_0, & x < 0 \\ h_1, & 0 < x < L \\ h_2, & x > L, \end{cases} \tag{3}$$

where h_0, h_1, and h_2 are distinct, real, and non-negative. This gives six canonical cases, which we denote as

$$\text{I}(\sqcap\!\!\sqcup\!\!\sqcap): \ h_0 > h_1 > h_2, \quad \text{II}(\sqcap\!\!\sqcup\!\!\sqcap): \ h_0 > h_2 > h_1,$$
$$\text{III}(\sqcup\!\!\sqcap\!\!\sqcup): \ h_1 > h_0 > h_2, \quad \text{IV}(\sqcup\!\!\sqcap\!\!\sqcap): \ h_2 > h_0 > h_1,$$
$$\text{V}(\sqcap\!\!\sqcup\!\!\sqcup): \ h_1 > h_2 > h_0, \quad \text{VI}(\sqcup\!\!\sqcap\!\!\sqcup): \ h_2 > h_1 > h_0,$$

where an icon of the initial step data is shown in parentheses. When convenient, and without loss of generality, we take h_i to be 0, 1 and $0 < h_* < 1$ (by using a scaling symmetry and Galilean invariance). The case of a well (e.g., $h_0 = h_2 = 0 > h_1$) and a box (e.g., $h_0 = h_2 = 0 < h_1$) with vanishing boundaries was studied in [7], where the asymptotic solution was constructed analytically.

This paper is organized as follows. We first discuss case I ($\sqcap\!\!\sqcup\!\!\sqcap$), where two DSWs interact and exhibit a two-phase region that evolves into effectively a one-phase solution for large time. Single-phase Whitham theory is then introduced to describe the DSW with a small amplitude wave train that develops in case II ($\sqcap\!\!\sqcup\!\!\sqcup$). We then briefly discuss multiphase Whitham theory to describe the two-phase region in case I ($\sqcap\!\!\sqcup\!\!\sqcap$). In case III ($\sqcup\!\!\sqcap\!\!\sqcup$), the interaction produces a DSW with a finite number of solitons, which remarkably can be determined analytically using inverse scattering transform (IST) theory (cf. [13]). There is no analog for emerging solitons in VSWs. We then use Whitham and IST theory to describe the interactions in cases IV ($\sqcup\!\!\sqcap\!\!\sqcap$), V ($\sqcap\!\!\sqcup\!\!\sqcup$), and VI ($\sqcup\!\!\sqcap\!\!\sqcup$). Finally, we comment on the numerical scheme we used to solve Eqs. (1) and (2).

In case I ($\sqcap\!\!\sqcup\!\!\sqcap$), two one-phase DSWs form and propagate to the right [see Fig. 1(a)]. When the shock front of the left DSW reaches the expanding oscillatory tail of the right DSW, they interact and form a quasiperiodic two-phase solution [see Fig. 1(b)]. The shock front of the left DSW subsequently overtakes the shock front of the right DSW and forms a one-phase solution to the right of the two-phase region [see Fig. 1(c)]. To the left of the two-phase solution, an essentially one-phase DSW tail emerges [see Fig. 1(c)]; although the tail is weakly modulated by a quasiperiodic wave, its behavior is essentially one-phase. For large time, the two-phase region closes and a one-phase DSW remains [see Figs. 1(d) and 1(e)]; Whitham theory indicates that the amplitude of the two-phase modulations decreases with time and results in an effectively one-phase DSW. This closing of the two-phase region is suggested by the rigorous (Whitham theory) results in [15], though the authors studied smooth initial data. The computation of the boundaries of the one- and two-phase regions using multiphase Whitham theory is discussed later in this paper.

*shockwaves@douglasbaldwin.com

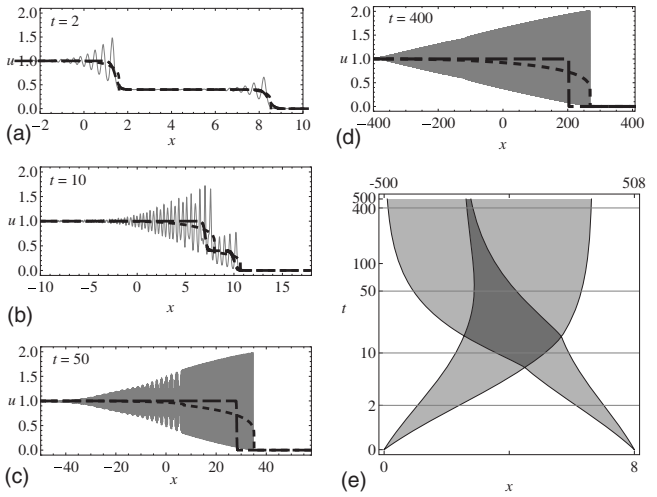

FIG. 1. Plots (a)–(d) show the numerically computed solution of Eq. (1) and (e) the boundary of the one- (light gray) and two-phase (dark gray) regions computed using Whitham theory. The averaged solution, $\bar{u}$, is computed using Whitham averaging (cf. [14]) and shown as dotted lines in (a)–(d); the solution of Eq. (2) with $\nu=\varepsilon$ is shown as dashed lines in (a)–(d). In all plots, $\varepsilon^2=0.001$, $h_0=1$, $h_1=0.4$, $h_2=0$, and $L=8$. The vertical axis in (e) is log-time and the horizontal axis is $-t\leq x\leq t+8$ [and matches the domain in (a)–(d)].

Although the (initial) shock front speed is different for DSWs and VSWs ($2h_0/3$ and $h_0/2$, respectively), the averaged DSWs are similar in behavior to VSWs [see Figs. 1(a)–1(d)]; in both, two shock waves merge to form a single shock wave.

For case II (⌐¬), a large DSW forms on the left and a small rarefaction wave (RW) forms on the right [see Fig. 2(a)]. The front of the DSW then interacts with the trailing edge of the RW; the interaction decreases the DSW's speed and height [see Fig. 2(b)]. The front of the DSW is faster than the front of the RW and overtakes it [see Fig. 2(c)]. The size of the interaction region continues to expand with a DSW emerging in front with a small amplitude wave train behind, whose amplitude is proportional to $t^{-1/2}$ [see Fig. 2(d)]. As in case I (⌐¬), the averaged DSW and the VSW (see Fig. 2) both tend to a single DSW (VSW) once the front of the DSW (VSW) passes the front of the RW.

We can use the one-phase Whitham equations to characterize the interaction of the DSW and RW in case II (⌐¬). In this context, Whitham theory consists of looking for a fully nonlinear single-phase or multiphase solution whose parameters (amplitude, wave number, and frequency) are slowly varying with respect to the phase(s) and then deriving new equations for the evolution of the slowly varying wave properties. The one-phase Whitham equations for Eq. (1) are [8]

$$\frac{\partial r_i}{\partial t}+v_i(r_1,r_2,r_3)\frac{\partial r_i}{\partial x}=0,\quad i=1,2,3, \tag{4a}$$

where

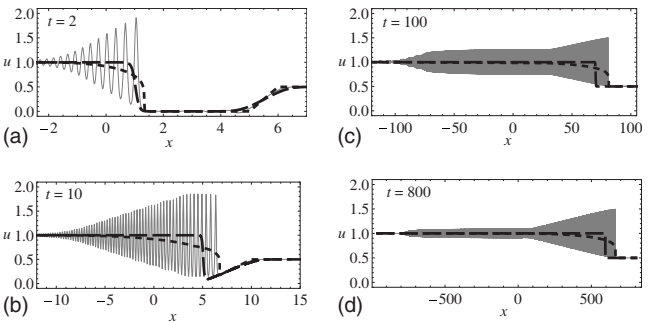

FIG. 2. Plots of the numerical and averaged Whitham solutions of Eq. (1) for case II (⌐¬), where $\varepsilon^2=0.001$, $h_0=1$, $h_1=0$, $h_2=0.5$, and $L=5$. Dotted lines correspond to $\bar{u}$ and the dashed lines correspond to the solution of Eq. (2).

$$v_1=V-\frac{2}{3}(r_2-r_1)\frac{K(m)}{K(m)-E(m)},$$

$$v_2=V-\frac{2}{3}(r_2-r_1)\frac{(1-m)K(m)}{E(m)-(1-m)K(m)},$$

$$v_3=V+\frac{2}{3}(r_3-r_1)\frac{(1-m)K(m)}{E(m)}, \tag{4b}$$

$V=(r_1+r_2+r_3)/3$, $m=(r_2-r_1)/(r_3-r_1)$, $K(m)$ is the complete elliptic integral of the first kind, and $E(m)$ is the complete elliptic integral of the second kind. Then, the asymptotic solution is

$$u_a(x,t)\approx r_1+r_2-r_3+2(r_3-r_1)\mathrm{dn}^2(K(m)\theta/\pi;m),$$

where $\theta_x=\kappa$, $\theta_t=-\omega=-\kappa V$, $\kappa=\pi\sqrt{(r_3-r_1)/(6\epsilon^2)}/K(m)$, and r_i are slowly varying functions of x and t. We can make a global dispersive regularization for the initial value problems (1) and (3) by choosing appropriate initial data for the r_i [3,16] that result in a global solution. A global dispersive regularization of case II (⌐¬) is shown in Fig. 3; the r_i are taken to be nondecreasing, $r_i(x,0)\leq r_{i+1}(x,0)$ where $r_i=r_{i+1}$ is interpreted in the limiting sense $r_i\to r_{i+1}$ and $\bar{u}_a(x,0)=u(x,0)$ for all $x\in\mathbb{R}$.

In order to study the interaction we evolve the r_i numerically. A simple and effective method for evolving the r_i is to discretize the initial data regularization along the dependent variable, r_i, and then compute the shift in x of each data point using Eq. (4). Figure 4 compares a numerically evolved Whitham approximation with direct numerics for case II (⌐¬); the first-order Whitham approximation does not capture the small quasiperiodic modulations in the tail because they are higher-order effects. Both direct numerics and the Whitham approximation agree and show that for large enough time, the amplitude of the tail in case II (⌐¬) is proportional to $t^{-1/2}$; this is typical of a uniform linear wave train when the total energy remains constant (cf. [10]) and was observed in the context of a well with vanishing boundaries (e.g., $h_0=h_2=0>h_1$) in [7]

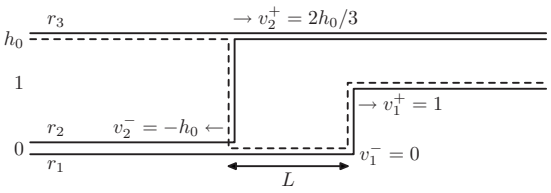

FIG. 3. The initial data regularization of case II ( ) for $h_0>1$, $h_1=0$, and $h_2=1$; the dashed line is the initial condition, $u_0(x)$, and the solid lines are r_1, r_2, and r_3. The figure also gives the speed of the front and back of the DSW and RW at $t=0$.

Multiphase Whitham theory is more complicated than one-phase Whitham theory and dates back to 1970 [17]; multiphase Whitham equations were developed for the KdV equation in [18]. The interaction of two DSWs from certain steplike data was recently analyzed in [6] for the nonlinear Schrödinger equation. The one- and two-phase regions and the averaged solution in case I ( ) are found by numerically evolving the two-phase Whitham equations for the KdV (see [14]),

$$\frac{\partial r_i}{\partial t} + v_i(r_1, \ldots, r_5)\frac{\partial r_i}{\partial x} = 0, \quad i = 1,2, \ldots, 5, \tag{5}$$

where $v_i=(2r_i^3-\chi r_i^2-\beta_1 r_i-\beta_2)/(r_i^2-\alpha_1 r_i-\alpha_2)$, $\chi=\Sigma_{j=1}^5 r_j$, and α_1, α_2, β_1, and β_2 are solutions of

$$\begin{bmatrix} I_1^1 & I_1^0 \\ I_2^1 & I_2^0 \end{bmatrix}\begin{bmatrix} \alpha_1 \\ \alpha_2 \end{bmatrix} = \begin{bmatrix} I_1^2 \\ I_2^2 \end{bmatrix}, \quad \begin{bmatrix} I_1^1 & I_1^0 \\ I_2^1 & I_2^0 \end{bmatrix}\begin{bmatrix} \beta_1 \\ \beta_2 \end{bmatrix} = \begin{bmatrix} 2I_1^3-\chi I_1^2 \\ 2I_2^3-\chi I_2^2 \end{bmatrix},$$

with

$$I_j^k = \int_{r_{2j-1}}^{r_{2j}} \frac{\xi^k}{\sqrt{(\xi-r_1)(\xi-r_2)(\xi-r_3)(\xi-r_4)(\xi-r_5)}} d\xi. \tag{6}$$

In case III ( ), a small RW forms on the left and a large DSW forms on the right. The front of the RW then interacts with the tail of the DSW and reduces the amplitude of the waves—essentially cutting off the top of the box. Since the front speed of the RW is less than the front speed of the initial DSW, a finite number of solitons can escape the interaction (see Fig. 5). These solitons have no analog in the VSW solution of case III ( ). We can compute the precise number, height, and speed of these escaping solitons for all time using IST theory.

From IST theory, the number of solitons correspond to the time-independent number of zeros of $a(k)$ [which is the number of poles of the reflection coefficient $R\equiv b(k)/a(k)$] in the upper half k plane. Associated with Eq. (1), the data $a(k)$ is defined by

$$\phi(x;k) \equiv a(k)\bar{\psi}(x;k) + b(k)\psi(x;k),$$

$$\bar{\phi}(x;k) \equiv \bar{a}(k)\psi(x;k) + \bar{b}(k)\bar{\psi}(x;k),$$

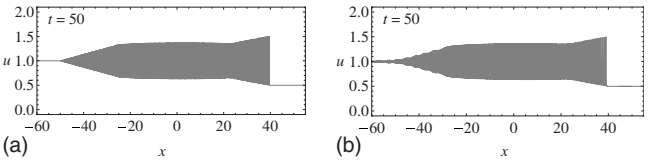

FIG. 4. Plot (a) shows the Whitham approximation and (b) direct numerics of the solution of Eq. (1) for case II ( ) with the same initial condition as Fig. 2.

corresponding to the eigenfunctions

$$\phi(x;k) \sim e^{-ik_0 x}, \quad \bar{\phi}(x;k) \sim e^{ik_0 x}, \text{ as } x \to -\infty,$$

$$\psi(x;k) \sim e^{ik_2 x}, \quad \bar{\psi}(x;k) \sim e^{-ik_2 x}, \text{ as } x \to +\infty,$$

which satisfy the Schrödinger scattering problem,

$$w_{xx} + w\{u/6 + k^2\}/\varepsilon^2 = 0. \tag{7}$$

The solution of Eq. (7), at $t=0$, with the potential u from Eq. (3), is

$$w(x) = \begin{cases} Ae^{ik_0 x} + Be^{-ik_0 x}, & x < 0 \\ Ce^{ik_1 x} + De^{-ik_1 x}, & 0 < x < L \\ Ee^{ik_2 x} + Fe^{-ik_2 x}, & x > L, \end{cases}$$

where $k_0=\sqrt{h_0/6+k^2}/\varepsilon$, $k_1=\sqrt{h_1/6+k^2}/\varepsilon$, and $k_2=\sqrt{h_2/6+k^2}/\varepsilon$. The eigenfunctions ϕ, $\bar{\phi}$, ψ, and $\bar{\psi}$ are determined by requiring that w and w' are continuous across $x=0$ and $x=L$. Indeed, ϕ is found by taking $A=0$ and $B=1$ and then solving for C, D, $E\equiv b(k)$, $F\equiv a(k)$, so that

$$a(k) = e^{ik_2 L}\frac{k_0+k_2}{2k_2}\left\{\cos(k_1 L) - i\frac{k_1^2+k_0 k_2}{k_1(k_0+k_2)}\sin(k_1 L)\right\}.$$

Note that the branch cut in $a(k)$ corresponds to the DSW in case III ( ) and the RW in case V ( ). Since $e^{ik_2 L}(k_0+k_2)/(2k_2)\neq 0$, the zeros of $a(k)$ occur when $\tan(k_1 L)=ik_1(k_0+k_2)/(k_1^2+k_0 k_2)$.

It can be shown that the zeros of $a(k)$ are purely imaginary; thus, we let $k=i\kappa$ (where $\kappa\in\mathbb{R}$ and $\kappa>0$). For case III ( ), where $h_1=1>h_0=h_*$ and $h_2=0$, the zeros of $a(i\kappa)$ occur when

$$\tan(\sqrt{1/6-\kappa^2}L/\varepsilon) = \frac{\sqrt{1/6-\kappa^2}(\sqrt{\kappa^2-h_*/6}+\kappa)}{1/6-\kappa^2-\kappa\sqrt{\kappa^2-h_*/6}}. \tag{8}$$

If we denote the zeros determined using Eq. (8) as $\kappa_1, \kappa_2, \ldots, \kappa_N$, then the corresponding solitons in case III ( ) have height $12\kappa_i^2$ and speed $4\kappa_i^2$. The number of periods for $\sqrt{h_*/6}\leq\kappa\leq\sqrt{1/6}$ of the right-hand side of Eq. (8), $L\sqrt{1-h_*}/(\varepsilon\pi\sqrt{6})$, is an estimate of the number of solitons. The number, height, and speed of the solitons determined using Eq. (8) exactly correspond to the solitons observed using direct numerics (for various values of h_*, L, and ε).

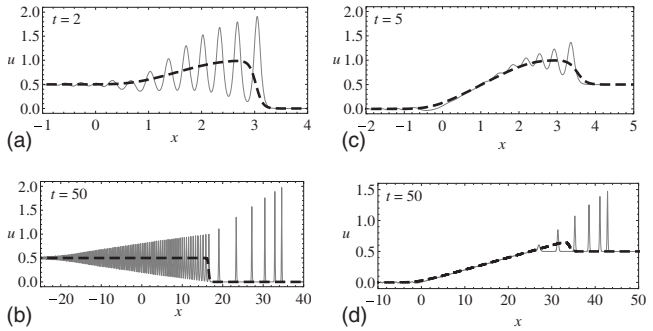

FIG. 5. Plots (a) and (b) show case III ( ) with $h_0=0.5$, $h_1=1$, $h_2=0$ and (c) and (d) show case V ( ) with $h_0=0$, $h_1=1$, $h_2=0.5$, where $\varepsilon^2=0.001$ and $L=2$. There are six solitons in both cases; see Eq. (8).

In case IV ( ), a small DSW forms on the left and a large RW forms on the right [see Fig. 6(a)]. As in case II ( ), the front of the DSW interacts with the trailing edge of the RW and decreases the DSW's amplitude and speed. Unlike case II ( ), the front of the DSW does not overtake the front of the RW. The DSW becomes a small amplitude tail on the left of the RW and decreases in amplitude proportional to $t^{-1/2}$ [see Fig. 6(b)].

For case V ( ), a large RW forms on the left and a small DSW forms on the right; the front of the RW interacts with the tail of the DSW and results in a RW and a finite number of solitons. The solitons correspond to the number of zeros of Eq. (8) where $h_0=0$ and $h_1=1>h_2=h_*$.

In case VI ( ), two rarefaction waves form; the small amplitude oscillatory tail [see, for instance, the RW in Fig. 6(a)] of the right RW interacts with the front of the left RW; the tails of the right and left RW then interact to form a small amplitude, modulated, quasiperiodic tail; this modulation decreases with time and case VI ( ) tends to a pure RW for large time.

We numerically solve Eqs. (1) and (2) using an adaptation of the modified exponential time-differencing fourth-order Runge-Kutta (ETDRK4) method (see [19]). When this numerical scheme was used to compute a known exact solution, it was accurate to more than six decimal digits.

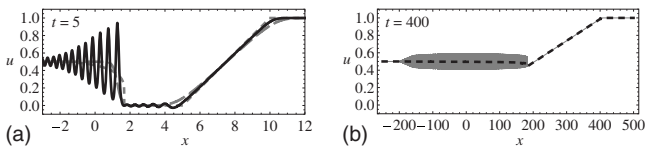

FIG. 6. Plots of the solution of Eq. (1) for case IV ( ), where $\varepsilon^2=0.001$, $h_0=0.5$, $h_1=0$, $h_2=1$, and $L=5$.

For spectral accuracy when using the ETDRK4 method, the initial data must be both smooth and periodic. Therefore, we differentiate Eq. (1) with respect to x and define $v\equiv u_x$ to get $v_t+(uv)_x+\varepsilon^2 v_{xxx}=0$. Transforming to Fourier space gives $\hat{v}_t=i\varepsilon^2k^3\hat{v}-ik\widehat{uv}\equiv\mathbf{L}\hat{v}+\mathbf{N}(\hat{v},t)$, where we define $(\mathbf{L}\hat{v})(k)\equiv i\varepsilon^2k^3\hat{v}$ and $\mathbf{N}(\hat{v},t)=\mathbf{N}(\hat{v})\equiv -ik\mathcal{F}\{[h_0+\int_{-\infty}^{x}\mathcal{F}^{-1}(\hat{v})dx']\mathcal{F}^{-1}(\hat{v})\}$. It is important that the integral in $\mathbf{N}$ is computed using a spectrally accurate method. Moreover, we approximate the initial step data with the analytic function $2wv(x,0)=(h_2-h_1)\mathrm{sech}^2[(x-L)/w]+(h_1-h_0)\mathrm{sech}^2(x/w)$, where w is small. See [19] for details about how this $\mathbf{L}$ and $\mathbf{N}$ are used to numerically compute the solution of Eq. (1).

For large time, cases I ( ) and II ( ) go to a single DSW, while cases IV ( ) and VI ( ) go to a single RW; this is consistent with VSW theory. However, unlike VSW theory, cases III ( ) and V ( ) form a finite number of solitons in addition to the DSW or RW, respectively. Moreover, unlike VSW theory, case I ( ) exhibits a transient two-phase region and cases II ( ) and IV ( ) have a small amplitude tail that decays at a rate proportional to $t^{-1/2}$.

This work was partially supported by NSF Grants No. DMS-0604151 and No. DMS-0803074, Air Force Office of Scientific Research Grant No. FA9550-09-1-0250, and NDSEG.

[1] R. J. Taylor, D. R. Baker, and H. Ikezi, Phys. Rev. Lett. **24**, 206 (1970).
[2] N. F. Smyth and P. E. Holloway, J. Phys. Oceanogr. **18**, 947 (1988).
[3] M. A. Hoefer, M. J. Ablowitz, I. Coddington, E. A. Cornell, P. Engels, and V. Schweikhard, Phys. Rev. A **74**, 023623 (2006).
[4] J. J. Chang, P. Engels, and M. A. Hoefer, Phys. Rev. Lett. **101**, 170404 (2008).
[5] W. Wan, S. Jia, and J. W. Fleischer, Nat. Phys. **3**, 46 (2007).
[6] M. A. Hoefer and M. J. Ablowitz, Physica D **236**, 44 (2007).
[7] G. A. El and R. H. J. Grimshaw, Chaos **12**, 1015 (2002).
[8] A. V. Gurevich and L. P. Pitaevskii, Sov. Phys. JETP **38**, 291 (1974).
[9] A. M. Kamchatnov, *Nonlinear Periodic Waves and Their Modulations* (World Scientific, River Edge, NJ, 2000); G. A. El, Chaos **15**, 037103 (2005).
[10] G. B. Whitham, Proc. R. Soc. London, Ser. A **283**, 238 (1965).
[11] G. B. Whitham, *Linear and Nonlinear Waves* (Wiley, New York, 1974).
[12] R. Courant and K. O. Friedrichs, *Supersonic Flow and Shock Waves* (Interscience, New York, 1948); P. D. Lax, *Hyperbolic Systems of Conservation Laws and the Mathematical Theory of Shock Waves* (SIAM, Philadelphia, 1973).
[13] M. J. Ablowitz and P. A. Clarkson, *Solitons, Nonlinear Evolution Equations, and Inverse Scattering* (Cambridge University Press, Cambridge, England, 1991).
[14] C. D. Levermore, Commun. Partial Differ. Equ. **13**, 495 (1988).

[15] T. Grava and F.-R. Tian, Commun. Pure Appl. Math. **55**, 1569 (2002).

[16] Y. Kodama, SIAM J. Appl. Math. **59**, 2162 (1999); G. Biondini and Y. Kodama, J. Nonlinear Sci. **16**, 435 (2006).

[17] M. J. Ablowitz and D. J. Benny, Stud. Appl. Math. **49**, 225 (1970).

[18] H. Flaschka, M. G. Forest, and D. W. McLaughlin, Commun. Pure Appl. Math. **33**, 739 (1980).

[19] A.-K. Kassam and L. N. Trefethen, SIAM J. Sci. Comput. **26**, 1214 (2005); S. M. Cox and P. C. Matthews, J. Comput. Phys. **176**, 430 (2002).